Design and Analysis of a High-Efficiency Resonant Converter for EV Battery Charger

Birand Erdogan*, Adnan Tan, Murat Mustafa Savrun, Mehmet Ugras Cuma and Mehmet Tumay

***Abstract*— The interest in electric vehicle (EVs) components such as battery, battery chargers, and battery management systems is increasing in parallel with the spread of electric vehicles. One of the most critical of these components is battery chargers. Battery chargers are equipped with DC-DC converters with high efficiency, low cost, and wide output voltage range. In order to provide reliable operation of the battery charger, it is of great importance that the DC-DC converters are operated with a robust and stable controller as well as designed optimally. In this paper, a design method for a CLLC resonant converter-based bidirectional dc-dc converter (BiDC) is presented for a battery charger. The resonant converter, whose design details are presented, suggests a resonant system to be used in battery chargers with fewer components than the CLLLC converter, and similar voltage gain characteristics for bidirectional power flow operations compared to the LLC converter. The design procedure highlights performing the soft switching operation and determining the resonant tank parameters. In addition, the forward mode and reverse mode gain equations required for the system to operate in the desired output voltage range have been presented. The design procedures have been validated with a CLLC BiDC model with ratings of 1 kW, 400 V input / 300-450 V output in the PSIM environment. The performance results reveal that the zero voltage switching (ZVS) has been performed for primary-side MOSFETs under a wide load range.**

Index Terms— **Battery chargers, CLLC resonant converter, high efficiency, DC-DC converter**

I. INTRODUCTION

With increasing electrical power demands, battery systems in electric vehicles, which are becoming increasingly common, can also be used as energy storage and auxiliary services.

BİRAND ERDOGAN, is with Department of the Electrical and Electronics Engineering of Adana Alparslan Türkeş Science and Technology University, Adana, Turkey,(e-mail: berdogan@atu.edu.tr).
https://orcid.org/0000-0003-0784-7776
ADNAN TAN, is with Department of the Electrical and Electronics Engineering of Çukurova University, Adana, Turkey, (e-mail: atan@cu.edu.tr).
https://orcid.org/0000-0002-5227-2556
MURAT MUSTAFA SAVRUN, is with Department of the Electrical and Electronics Engineering of Adana Alparslan Türkeş Science and Technology University, Adana, Turkey, (e-mail: msavrun@atu.edu.tr).
https://orcid.org/0000-0001-5847-5082
MEHMET UGRAS CUMA, is with Department of the Electrical and Electronics Engineering of Çukurova University, Adana, Turkey, (e-mail: mcuma@cu.edu.tr).
https://orcid.org/0000-0001- 6040-0362
MEHMET TUMAY, is with Department of the Electrical and Electronics Engineering of Çukurova University, Adana, Turkey, (e-mail: mtumay@cu.edu.tr).
https://orcid.org/0000-0003-2938-8005

Manuscript received October 23, 2021; accepted December 22, 2022.
DOI: 10.17694/bajece.1013720

Grid-integrated electric vehicles are promising technologies for smart grids and reducing the environmental impact of vehicles. This technology is named as vehicle-to-grid concept (V2G) [1-3]. With the V2G concept, which emerged with the spread of distributed generation, EV batteries can transfer power to home loads or to the grid. Considering that EVs are parked for an average of 8 hours a day, in the event of a grid outage and high electricity prices, EVs can be used as a resource, reducing outages and the cost of electricity usage. Thus, bidirectional battery chargers (BCs) are frequently used instead of unidirectional BCs in such applications. The general structure of BC is shown in Fig. 1. BiDCs are used to provide transmission between high voltage buses and low voltage buses. Unlike resonant [4]–[6] or PWM [7]–[9] model unidirectional converters, BiDCs are designed by replacing output rectifiers with MOSFET switches. There are several studies on BiDCs that have soft-switching capability (SSC) with a focus on eliminating the switching loss. The related studies emphasize that BiDCs can be operated at high frequency-high power density without sacrificing efficiency [10-15]. BiDC topologies are divided into isolated and non-isolated, and isolated topologies stand out due to their safety [16] and flexible voltage range. Isolated topologies are divided into two as phase shift method and frequency control methods in resonant structure. The phase shift control method can be used for isolated BiDCs but the gain of the system for this method is limited. In addition, SSC is a problem when the system is operating with a wide load range [17]. The resonant tank, which is frequently used in isolated BiDCs, achieves high gain values as well as performing soft switching in a wide load range. LLC resonant converter is an isolated dc-dc converter that has SSC for a wide load range at the secondary side [18-22]. However, the drawback of the LLC resonant converter is that the voltage gain characteristics it provides in the forward direction cannot be provided in the reverse direction. While the LLC resonant converter's normalized gain is 1 in forward power flow, the converter's normalized gain is lower than 1 in reverse power flow. This drawback has been able to eliminate by using a symmetric resonant tank structure such as CLLLC [23-26]. The restriction of the CLLLC resonant converter is that there are too many components which is a problem in designing/analyzing the converter and it is also not cost-effective. In order to have a symmetric tank structure and fewer components than CLLLC, CLLC resonant converter is proposed in the literature [17, 27]. One of the advantages of CLLC topology is that the resonant

inductor on the secondary side of the CLLLC converter is removed and that makes the circuit easier to design. Another advantage is that similar voltage gain characteristics are observed in both directions in CLLC topology which is not seen in LLC resonant converter. The different types of resonant converter topologies used in literature are illustrated in Fig. 2.

In this paper, the high-efficiency resonant converter is presented for BCAs. The contribution of the paper is that the design procedure is improved by considering the reverse side initially so the complexity of designing the system is reduced in comparison with the literature. In addition, CC-CV charging control algorithms are implemented to verify the performance of the battery charger with bidirectional power flow capability which is significant for V2G concept, and these control methods are expressed mathematically. This paper is divided into five sections. In the first section, literature studies on resonant converter topologies are presented. In the second section, resonant converter topology is explained. In the third section, the design procedure and control algorithm is presented. In section 4, simulation results are given for both modes. The last section presents the concluding remarks of the paper.

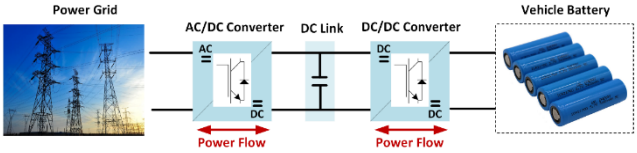

Fig.1. General Structure of BC

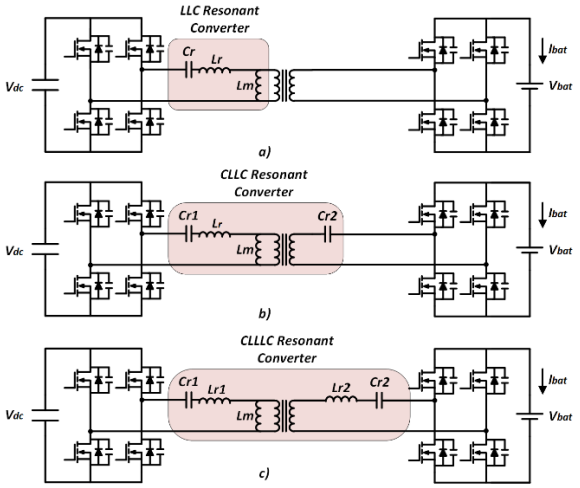

Fig.2. Resonant Converter Topologies a) LLC resonant converter b) CLLC resonant converter c) CLLLC resonant converter

II. CLLC RESONANT CONVERTER

In this study, a full-bridge resonant CLLC converter topology, which is illustrated in Fig. 3, is used for BiDC due to high power ratings, similar voltage gain characteristics, and less volume. V_{in} stands for the input voltage of the proposed system. M_1 – M_4 are the primary MOSFETs. L_r, C_{r1} and L_m, that are the resonant inductor, primary side resonant capacitor, and the magnetizing inductor, respectively, are the crucial resonant tank elements of the primary side. Additionally, C_{r2} stands, that is the secondary side resonant capacitor, is the fundamental resonant tank element of the secondary side. Turn ratio of the transformer is denoted as n. R_{o1} and R_{o2} are the load resistors of forward and reverse modes, respectively. M_5-M_8 are secondary side MOSFETs. C_1 and C_2 are the capacitors of input and output parts. First of all, first harmonic approximation method is applied to investigate the working principle of the converter, and determine the transfer function of the resonant tank gain by using the AC equivalent circuit of the system. The AC equivalent circuits of the forward and reverse modes are depicted in Fig. 4. R_{ac_f} is the equivalent of the reflected load resistance represented in Eq-1 for forward mode. Addition to that, R_{ac_r} (the equivalent of the reflected load resistance) is also determined by virtue of reverse mode and outlined in Eq.2. To better understand, all aforementioned circuit parameters are tabulated in Table-1.

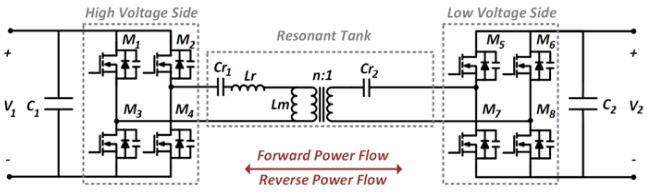

Fig.3. Bidirectional CLLC resonant converter topology

$$R_{ac\_f} = \frac{8n^2 R_{o1}}{\pi^2} \quad (1)$$

$$R_{ac\_r} = \frac{8R_{o2}}{\pi^2} \quad (2)$$

TABLE I
THE DEFINITIONS OF CIRCUIT PARAMETERS

Parameter	Expression	Meaning
Q_1	$\frac{\sqrt{L_r/C_{r1}}}{R_{ac\_f}}$	Quality factor of the forward mode
Q_2	$\frac{\sqrt{L_r/C_{r2n}}}{R_{ac\_r}}$	Quality factor of the reverse mode
C_X	$\frac{C_{r2n}}{C_{r1}}$	Ratio of resonant capacitors
L_X	$\frac{L_m}{L_r}$	Ratio of resonant inductors
C_{r2n}	$\frac{C_{r2}}{n^2}$	Normalized Capacitor of C_{r2}
F_x	$\frac{1}{2\pi\sqrt{L_r C_{r1}}}$	Basic Frequency
F_n	$\frac{F_s}{F_x}$	Normalized Frequency

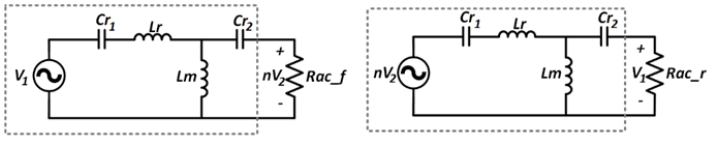

Fig.4. Equivalent Resonant Circuits a) Forward Mode b) Reverse Mode

Based on first harmonic approximation method transfer function of the resonant tank gain for both directions are shown below [17].

$$|G_f| = |\frac{nV_2}{V_1}| = \frac{1}{\sqrt{(\frac{L_x f^2 - 1 + f^2}{L_x f^2})^2 + (\frac{Q_1[C_x L_x f^4 - (C_x L_x + L_x + 1) f^2 + 1]}{C_x L_x f^3})^2}} \quad (3)$$

$$|G_r| = |\frac{V_1}{nV_2}| = \frac{1}{\sqrt{(\frac{C_x L_x f^2 - 1}{C_x L_x f^2})^2 + (\frac{Q_2[C_x L_x f^4 - (C_x L_x + L_x + 1) f^2 + 1]}{L_x f^3 \sqrt{C_x}})^2}} \quad (4)$$

As it is seen from above equations, dc gain of the BiDC depends on Q_1, Q_2, C_n, L_n and f. In section 3, design procedure of these parameters are clarified in detail. The crucial parameters namely SSC plays a vital role to improve the efficiency of the any desired systems. Due to the challenging design of SSCs, several restriction criteria should be considered during the analysis and design procedure. In the rest of this section, zero voltage switching (ZVS) boundaries, which take part in primary-side MOSFETs, are explained to minimize the energy losses. ZVS occurs when parasitic capacitors (PrCrs) are fully charged/discharged within desired duration namely dead-time.

The fundamental abbreviations of ZVS condition is outlined in Table 2. Determining the initial primary side current is required for SSC. According to the first harmonic approximation method for forward mode, the current is depicted in equation 5.

$$\mathrm{I_{dead\_f}} = \frac{1}{2}\int_O^{t_1} n\frac{v_2 - u_{cr2}}{L_m} dt, u_{cr2} = U_{cr2}\cos(2\pi f_s t + \theta) \quad (5)$$

For the secondary side, initial current is zero (see eq. 6).

$$\mathrm{i_{cr2}} = \mathrm{C_{r2}}\frac{du_{Cr2}}{dt}, \mathrm{i_{cr2}}(0) = 0 \quad (6)$$

From these two equations, current within dead-time in forward mode can be expressed as follows [17, 28-32].

$$\mathrm{I_{dead\_f}} = \frac{nV_2 t_1}{2L_m} \approx \frac{nV_2}{4f_s L_m} \quad (7)$$

To satisfy the ZVS condition for forward mode, Equation 8 is presented [17, 28-32].

$$\frac{\mathrm{I_{dead\_f}} t_{\mathrm{dead}}}{C_{eq\_f}} > \Delta u_{AB} = 2V_1 \quad (8)$$

Similar analysis can be done for the opposite direction. According to the first harmonic approximation method for reverse mode, $\mathrm{I_{dead\_r}}$ is shown in equation 9.

$$\mathrm{I_{dead\_r}} = \frac{1}{2}\int_O^{t_1} \frac{v_1 - u_{cr1} - u_{Lr}}{L_m} dt, u_{cr1} = U_{cr1}\cos(2\pi f_s t + \theta) \quad (9)$$

Similar to the forward mode, initial secondary side current is zero (see eq. 10).

$$\mathrm{i_{Lr}} = \mathrm{C_{r1}}\frac{du_{Cr1}}{dt}, \mathrm{u_{Lr}} = \mathrm{L_r}\frac{d\mathrm{i_{Lr}}}{dt}, \quad \mathrm{i_{Lr}}(0) = 0 \quad (10)$$

From these two equations, current within dead-time in reverse mode can be expressed as follows [17, 28-32].

$$\mathrm{I_{dead\_r}} = \frac{V_1 t_1}{2L_m} \approx \frac{V_1}{4f_s L_m} \quad (11)$$

To satisfy the ZVS condition for reverse mode, Equation 12 is presented [17, 28-32].

$$\frac{\mathrm{I_{dead\_r}} t_{\mathrm{dead}}}{C_{eq\_r}} > \Delta u_{CD} = 2nV_2 \quad (12)$$

TABLE II
THE ABBREVIATIONS OF CIRCUIT PARAMETERS FOR ZVS CONDITION

Parameter	Expression	Meaning
C_1, C_2, C_3, C_4	C_{oss1}	Parasitic capacitance of primary side MOSFETs
C_5, C_6, C_7, C_8	C_{oss2}	Parasitic capacitance of secondary side MOSFETs
C_{eq_f}	$C_{oss1} + \frac{C_{oss2}}{n^2}$	Equivalent capacitance of primary side in forward mode
C_{eq_r}	$C_{oss1} + \frac{C_{oss2}}{n^2}$	Equivalent capacitance of secondary side in reverse mode
I_{dead_f}	$\frac{nV_2}{4f_s L_m}$	Constant current for primary side in dead-time (forward mode)
I_{dead_r}	$\frac{V_1}{4f_s L_m}$	Constant current for secondary side in dead-time(reverse mode)
u_{cr2}	$U_{cr2}\cos(2\pi f_s t + \theta)$	Peak voltage on C_{r2}

III. DESIGN PROCEDURE, OPERATING PRINCIPLES AND CONTROL SCHEME

A. *Design Procedure*

In this paper, the novel design method is presented for BCAs. The design parameters based on the battery charger rating are outlined in Table 3. The proposed design procedure is expressed by a flowchart given in Fig. 5. The rating parameters of the CLLC circuit are initially determined before analyzing the proposed method.

TABLE III
DESIGN SPECIFICATIONS

Power Flow Direction	Max. Power	Primary side V1(V)	Secondary Side V2(V)	Switching Frequency Range
Forward	1kW	400	300-450	180-310 kHz
Reverse	1kW	300-450	400	170-260 kHz

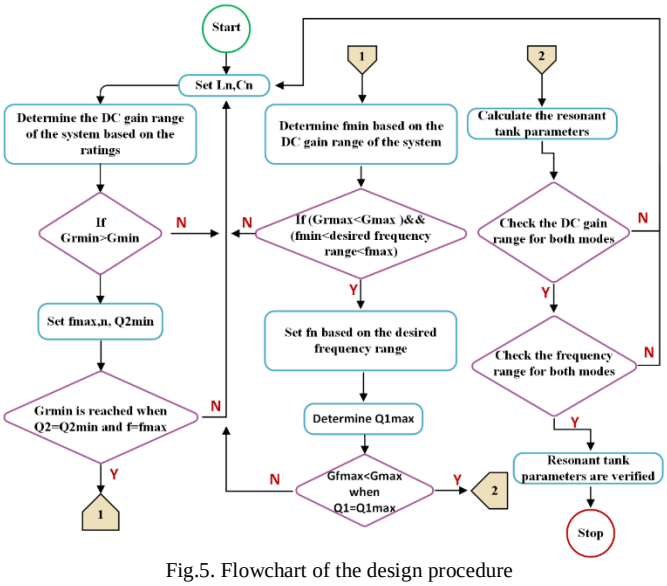

Fig.5. Flowchart of the design procedure

The design procedure initiates with the selecting L_n and C_n values. Following that, the fundamental performance parameters, which are maximum (G_{max})/minimum (G_{min}) DC voltage gain, forward/reverse mode gain range of the system, are determined according to the battery charger ratings. Since the design accuracy performed by considering the reverse mode is higher than the forward mode, the forward mode design is performed following the reverse mode design and the proposed method is started by checking if the minimum reverse mode gain is greater than G_{min} or not. Maximum normalized frequency, and the minimum quality factor are selected based on the G_{min} in reverse mode. When Q_2 reaches its designed minimum Q_{2min} and $f=f_{max}$, G_{min} is obtained. After determining fmax, fmin is obtained from DC gain range of the system. If f_{min} and f_{max} satisfy the desired DC gain range, normalized frequency is set based on the desired frequency range which is 150-350 kHz. Determining the Q_{1max} is important because of satisfying the condition for forward mode ($G_{fmax} < G_{max}$). After verifying all the conditions, the resonant tank parameters are able to be computed based on the ZVS equations which are shown in Eq. 8 and Eq. 12. Finally, the DC gain range for both modes and frequency range for both modes are checked before validating the resonant tank parameters. If any problem occurs during the design procedure, the parameters L_n and C_n are changed to meet the design requirements of the system, and the design procedure is restarted from the beginning. Fig. 6 shows the forward and reverse DC gain curve of the system with the initial guess of L_n=3 and C_n=1.3.

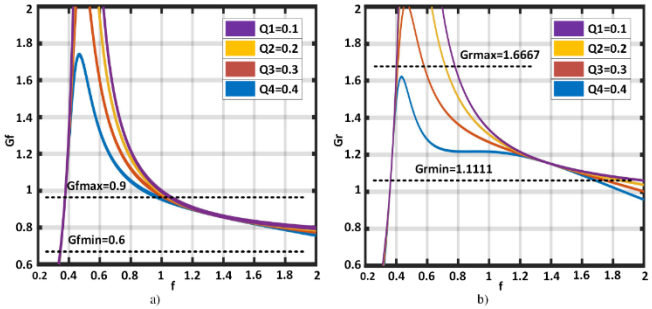

Fig.6. DC gain curves with different Quality Factors a) Forward mode b) Reverse mode

B. *Operating Principles*

The operating stages of the circuit is shown in Fig. 7. As illustrated in the figure, the converter has six operating stages during one switching cycle. While stages 1, 2, and 3 are performed in the first half cycle, stages 4, 5, and 6 are performed in the second half cycle. The converter operates within dead-time periods at stage 1 and 4. Stage 2 and 5 corresponds to resonant stages named power transfer stages. The converter operates out of resonance at stages 3 and 6. When the power transfer occurs, primary switches are triggered in inverting mode and the secondary side switches are disabled. Definitions of the converter stages are summarized in Table 4.

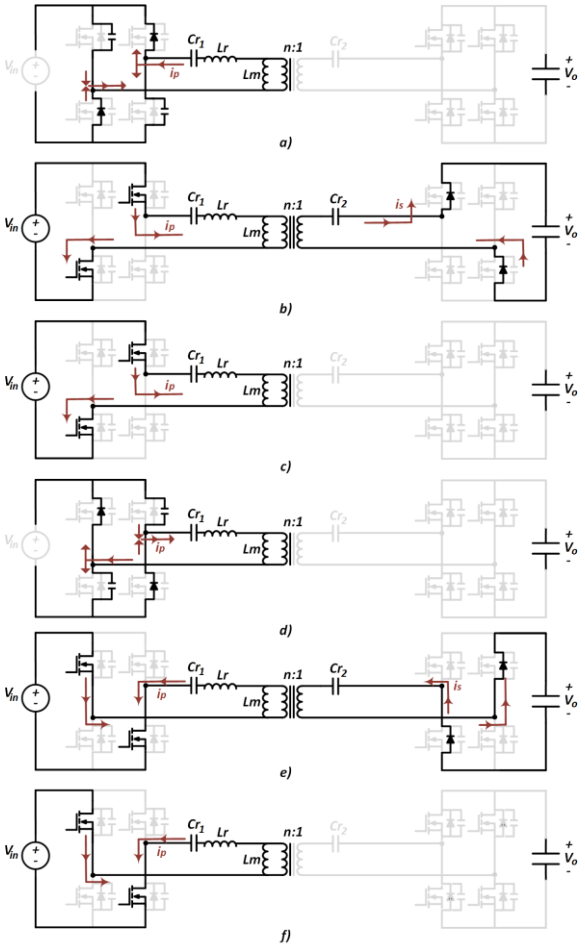

Fig.7. Operating Stages of the Resonant Converter a) Stage 1, b) Stage 2, c) Stage 3, d) Stage 4, e) Stage 5, and f) Stage 6.

TABLE IV
THE OPERATING PRINCIPLES OF THE CONVERTER

Stages	Explanation
Stage 1	Dead-time duration
Stage 2	Power is transferred to the secondary side
Stage 3	Out of resonance, power transfer is stopped
Stage 4	Dead-time duration
Stage 5	Power is transferred to the secondary side
Stage 6	Out of resonance, power transfer is stopped

C. Control Scheme

The cascade loop control scheme, designed for CC-CV charging algorithms for battery chargers, consists of the inner current control loop and the outer voltage control loop as represented in Fig. 8. Pulse frequency modulation is used for controlling the system.

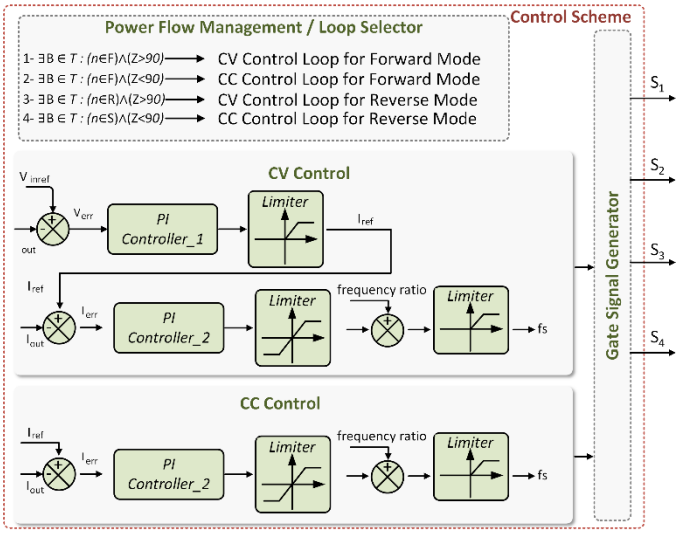

Fig.8. Block diagram of the CLLC resonant converter control system

Mathematical expressions are also shown in Fig. 8. As seen from Fig. 8, a power transfer process is defined by T. Bidirectional power flow capability B= F x S formed by forward mode and reverse mode. The measured SOC value is denoted as Z. As expressed in the figure, state 1 indicates that the CLLC converter operates in forward mode and the SOC level of the battery pack is more than 90 so CV control loop is selected by the control unit. Similarly, if the CLLC converter operates in forward mode but the SOC level of the battery pack is less than 90, the CC control loop is selected (state 2). SOC level in the battery pack that is more than 90 in state 3. The difference between state 1 and state 3 is that the converter operates in reverse mode at state 3, a CV control loop. Similar to state 3, the converter operates in reverse mode at state 4. However, the SOC level of the battery pack is less than 90 at state 4 so the CC control loop is selected by the control unit. CC charging is activated when the SOC is smaller than 90 percent. Similarly, CV charging is activated when the SOC is greater than 90 percent. For calculating the SOC value, SOC estimation methods can be used for real BCAs. However, in the simulation model, SOC value is directly measured from batteries so the SOC estimation method is not used in this paper. SOC value is taken and the control unit of the system decides whether CC or CV charge is required. Thus, the necessary signal is transmitted to the switch block. The reference voltage and reference current are denoted as V_{ref} and I_{ref}, respectively. In CC charging process, the difference between I_{ref} and the I_o generates a signal and enters the PI_2 controller for generating a duty cycle D when the Switch is OFF. The signal from the PI_2 controller is extracted from the calculated constant value and enters the limiter block that has upper/lower limits to generate the required switching frequency. The switching signals of MOSFEETs are produced by a gate signal generator considering the computed switching frequency. In the CV charging process (the switch is ON), the difference between V_{ref} and output voltage generates a signal and enters the PI_1 controller to be used in the inner loop. The remaining process is the same as in CC.

To summarize the control part, if the SOC value in the battery is below 90 percent while power is transferred from one side to another, the CC charging algorithm is used. CC control loop produces a frequency signal by comparing the measured battery charging current and reference current values and applying the error value to the PI controller. However, if the SOC value in the battery is above 90 percent, the CV charging algorithm is used. The CV control loop produces a reference signal by comparing the measured battery voltage with the reference voltage values and applying the error value to the PI controller. Similarly, this reference signal is compared with the battery current and the error value is applied to another PI controller to output a frequency signal. While CC and CV charging algorithms are used in the resonant converter, frequency control is performed and PI controllers, frequency ratio block and limiters are used to obtain necessary frequencies. The obtained frequency values are converted into switching signals by gate signal generator block.

IV. SIMULATION RESULTS

This section presents the performance review of the proposed system. A 1 kW battery charger model was developed using the PSIM simulation program. To examine the performance of the system, analyzes were carried out in all power flow directions and the functionality and applicability of the proposed battery charger were verified. Resonant tank design component values are shown in Table 5.

TABLE V
THE PARAMETERS OF SIMULATION MODEL

Parameter	Symbol	Value
Primary side Resonant Capacitor	Cr1	25 nF
Resonant Inductor	Lr	37.84 µH
Magnetic Inductor	Lm	57 µH
Secondary side Resonant Capacitor	Cr2	40 nF
Transformer Turn Ratio	n	8/10

All the design parameters are calculated based on the proposed design methodology discussed in sections 2 and 3. Simulation results show that the switching frequency range is between 180 kHz and 310 kHz which is the desired value for this system in forward mode (see Fig. 9). Similarly, the switching frequency range is between 170 kHz and 260 kHz in the reverse mode (see Fig. 10).

In forward mode, ZVS waveforms for maximum and minimum switching frequency are shown in Fig. 8. As seen

from the zoom-in view in the figure, the drain-to-source voltage of MOSFET is zero before the gate signal is equal to 1. Therefore, when the switch is turned on, the switching loss is zero. Similar to the Fig. 9, ZVS waveforms for maximum and minimum switching frequency are shown in Fig. 10 for reverse mode and ZVS is also seen from the zoom-in view in Fig. 10. Since zero voltage switching occurs, the switching losses are reduced, and the system's efficiency has increased compared to the traditional converters. The operating ranges of the system in both modes are highlighted in Fig. 9 and 10 by measuring the one period of the cycle.

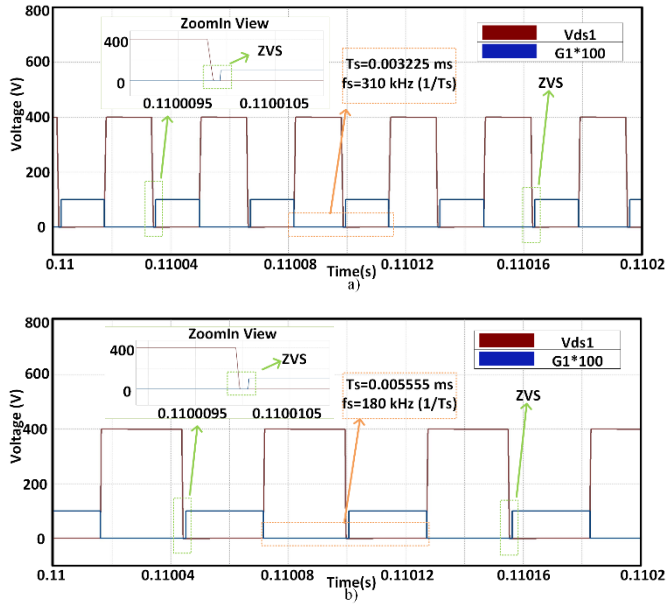

Fig. 9. ZVS waveforms for forward mode a) Maximum switching frequency b) Minimum switching frequency

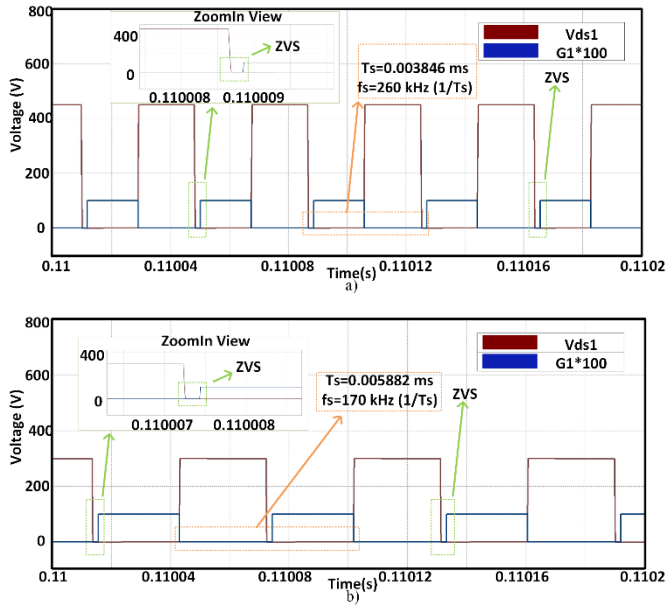

Fig.10. ZVS waveforms for reverse mode a) Maximum switching frequency b) Minimum switching frequency

As can be seen in Fig. 11, during the forward mode operation, the recommended frequency control is performed at 400 V input voltage, and an output voltage range of 300-450 V is obtained. While the output voltage is 450 V at the minimum operating frequency of 180 kHz, it reaches 300 V at the maximum operating frequency of 310 kHz. Similarly, when the system is operating in reverse mode (see Fig. 12), the desired 300-450 V output voltage range can be obtained by the PFM control method (for 400 V input). While the desired output voltage is obtained in reverse mode, the frequency range used in forward mode can be used. For instance, when the switching frequency is 260 kHz, output voltage is 450 V. On the other hand, when the switching frequency is 170 kHz, output voltage is 300 V.

In addition, switching losses and conduction losses of primary side MOSFETs are shown in Fig. 13 and Fig. 14, respectively. As seen in Fig. 13 and Fig. 14, the conduction losses are negligible. The main problem in this system comes from the switching losses as seen in Fig. 13 and Fig. 14. To overcome this problem (decrease switching loss), soft switching conditions are mentioned in the design procedure and simulation results confirm that the system has the soft-switching capability to reduce the switching losses (see Fig. 9 and Fig. 10).

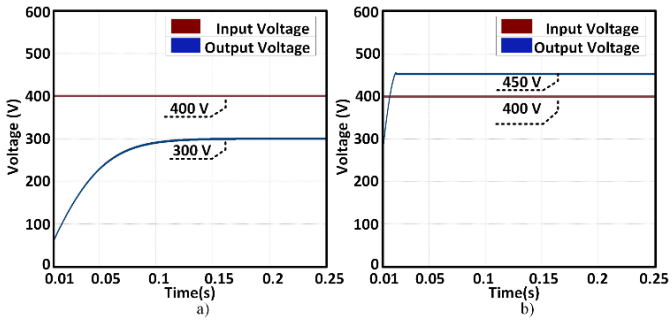

Fig.11. Input and output waveforms for forward mode a) System with maximum frequency b) System with minimum frequency

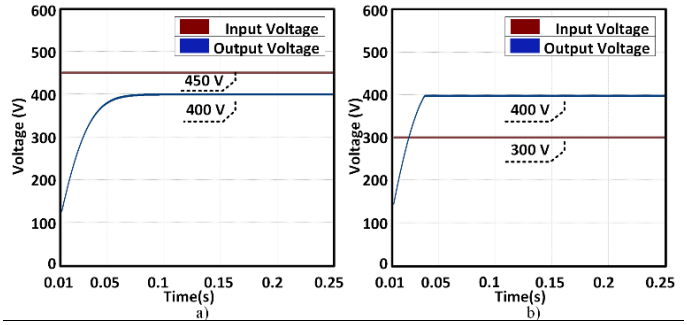

Fig.12. Input and output waveforms for reverse mode a) System with maximum frequency b) System with minimum frequency

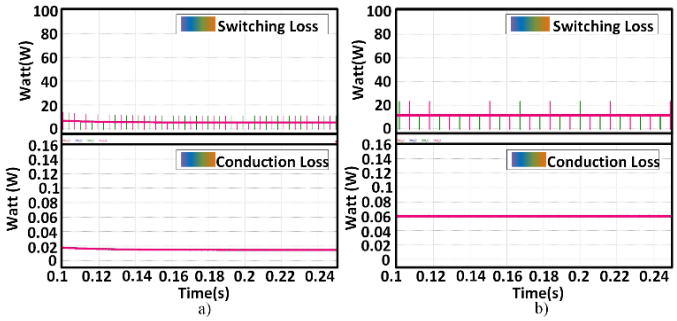

Fig.13. Switching and conduction losses for forward mode a) System with maximum frequency b) System with minimum frequency

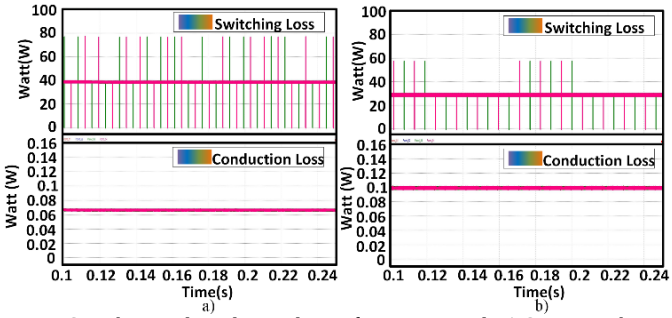

Fig.14. Switching and conduction losses for reverse mode a) System with maximum frequency b) System with minimum frequency

Results of the simulation model is shown in table 6. For a BCA, wide output load range is needed, and simulation results verified that the system has wide output load range for both modes (300 V-450 V) for a constant input voltage (400 V). Similar switching frequency range can used for the system with output power of 1 kW. Similar switching frequency range is used for both directions and the system has 1kW output power. Switching losses and conduction losses are acceptable for a 1kW system. When the resonant converter operates at 180 kHz and 310 kHz in forward mode, efficiency of the converter is 98.35 and 97.58, respectively. Similarly, the converter efficiency is 98.02/97.45 for 170 kHz/260 kHz in reverse mode.

TABLE VI
RESULTS OF SIMULATION MODEL

Parameter	Value
Input Voltage for two Modes	400 V
Output Voltage range for two Modes	300-450 V
Switching Loss for Forward Mode	15 W
Conduction Loss for Forward Mode	0.04 W
Switching Loss for Reverse Mode	35 W
Conduction Loss for Reverse Mode	0.04 W
Operating Frequency for Forward Mode	180 kHz – 310 kHz
Operating Frequency for Reverse Mode	170 kHz – 260 kHz
Output Power	1 kW

V. CONCLUSION

In this paper, a design method for CLLC resonant converter that is used in BCs is presented. To increase the efficiency of the system, soft switching conditions are given in design procedure. The simulation model of the resonant converter system which consists of two resonant capacitors, one resonant inductor, and one magnetizing inductor is performed using PSIM environment. Simulation model operates under wide output voltage range for a constant input voltage with rated power of 1 kW and also the model can transfer the power flow for both directions. CV and CC charging algorithms have been tested for the model with cascaded loop control and to control the output voltage to the desired value, PFM method is used. The presented system excels with the advantages of fewer components, less complexity, bidirectional power flow capability, and similar voltage gain characteristics for both directions in comparison with existing systems. In addition, another advantage of the presented system is that the converter satisfies a wide voltage range without sacrificing efficiency which is significant for BCAs. The main advantages of the presented topology are as follows:

- high efficiency,
- high energy density,
- electrical isolation,
- low electromagnetic interference and harmonic pollution,
- magnetic integration,
- wide output ranges,
- low voltage stress, and
- high operation frequency.

REFERENCES

[1] J. Chen, Y. Zhang and W. Su. "An anonymous authentication scheme for plug-in electric vehicles joining to charging/discharging station in vehicle-to-Grid (V2G) networks." in China Communications, vol. 12, no. 3, Mar. 2015, pp. 9-19, doi: 10.1109/CC.2015.7084359.

[2] S. Amamra and J. Marco. "Vehicle-to-Grid Aggregator to Support Power Grid and Reduce Electric Vehicle Charging Cost." in IEEE Access, vol. 7, 2019, pp. 178528-178538, doi: 10.1109/ACCESS.2019.2958664.

[3] M. A. Masrur, A. G. Skowronska, J. Hancock, S. W. Kolhoff, D. Z. McGrew, J. C. Vandiver, and J. Gatherer. "Military-Based Vehicle-to-Grid and Vehicle-to-Vehicle Microgrid—System Architecture and Implementation." in IEEE Transactions on Transportation Electrification, vol. 4, no. 1, March 2018, pp. 157-171, doi: 10.1109/TTE.2017.2779268.

[4] B. Ray. "Bidirectional DC/DC power conversion using constant-frequency quasi-resonant topology." 1993 IEEE International Symposium on Circuits and Systems, vol.4, 1993, pp. 2347-2350, doi: 10.1109/ISCAS.1993.394234.

[5] D. Ha, N. Park, K. Lee, D. Lee and D. Hyun. "Interleaved Bidirectional DC-DC Converter for Automotive Electric Systems." 2008 IEEE Industry Applications Society Annual Meeting, 2008, pp. 1-5, doi: 10.1109/08IAS.2008.291.

[6] H. Li, F. Z. Peng and J. S. Lawler. "A natural ZVS medium-power bidirectional DC-DC converter with minimum number of devices." in IEEE Transactions on Industry Applications, vol. 39, no. 2, March-April 2003, pp. 525-535, doi: 10.1109/TIA.2003.808965.

[7] K. W. Ma and Y. S. Lee. "An integrated flyback converter for DC uninterruptible power supply." in IEEE Transactions on Power Electronics, vol. 11, no. 2, March 1996, pp. 318-327, doi: 10.1109/63.486182.

[8] P. Das, B. Laan, S. A. Mousavi and G. Moschopoulos. "A Nonisolated Bidirectional ZVS-PWM Active Clamped DC–DC Converter." in IEEE Transactions on Power Electronics, vol. 24, no. 2, Feb. 2009, pp. 553-558, doi: 10.1109/TPEL.2008.2006897.

[9] D. Xu, C. Zhao and H. Fan. "A PWM plus phase-shift control bidirectional DC-DC converter." in IEEE Transactions on Power Electronics, vol. 19, no. 3, May 2004, pp. 666-675, doi: 10.1109/TPEL.2004.826485.

[10] L. Zhu. "A Novel Soft-Commutating Isolated Boost Full-Bridge ZVS-PWM DC–DC Converter for Bidirectional High Power Applications." in IEEE Transactions on Power Electronics, vol. 21, no. 2, March 2006, pp. 422-429, doi: 10.1109/TPEL.2005.869730.

[11] E. Hiraki, K. Yamamoto, T. Tanaka and T. Mishima. "An Isolated Bidirectional DC-DC Soft Switching Converter for Super Capacitor Based Energy Storage Systems." 2007 IEEE Power Electronics Specialists Conference, 2007, pp. 390-395, doi: 10.1109/PESC.2007.4342018.

[12] G. Ma, W. Qu, G. Yu, Y. Liu, N. Liang and W. Li. "A Zero-Voltage-Switching Bidirectional DC–DC Converter With State Analysis and Soft-Switching-Oriented Design Consideration." in IEEE Transactions on Industrial Electronics, vol. 56, no. 6, June 2009, pp. 2174-2184, doi: 10.1109/TIE.2009.2017566.

[13] H. Xiao and S. Xie. "A ZVS Bidirectional DC–DC Converter With Phase-Shift Plus PWM Control Scheme." in IEEE Transactions on Power Electronics, vol. 23, no. 2, March 2008, pp. 813-823, doi: 10.1109/TPEL.2007.915188.

[14] L. Schuch, C. Rech, H. L. Hey, H. A. Grundlinggrundling, H. Pinheiro and J. R. Pinheiro. "Analysis and Design of a New High-Efficiency Bidirectional Integrated ZVT PWM Converter for DC-Bus and Battery-Bank Interface." in IEEE Transactions on Industry Applications, vol. 42, no. 5, Sept.-Oct. 2006, pp. 1321-1332, doi: 10.1109/TIA.2006.880847.

[15] F. Z. Peng, Hui Li, Gui-Jia Su and J. S. Lawler. "A new ZVS bidirectional DC-DC converter for fuel cell and battery application." in

IEEE Transactions on Power Electronics, vol. 19, no. 1, Jan. 2004, pp. 54-65, doi: 10.1109/TPEL.2003.820550.
[16] S. Inoue and H. Akagi. "A Bidirectional DC–DC Converter for an Energy Storage System With Galvanic Isolation." in IEEE Transactions on Power Electronics, vol. 22, no. 6, Nov. 2007, pp. 2299-2306, doi: 10.1109/TPEL.2007.909248.
[17] Y. Liu, G. Du, X. Wang and Y. Lei. "Analysis and Design of High Efficiency Bidirectional GaN-Based CLLC Resonant Converter." in Energies, vol. 12, no. 20, Oct. 2019, pp. 3859-3871, doi:10.3390/en12203859
[18] Y. Wei, Q. Luo and A. Mantooth. "Comprehensive analysis and design of LLC resonant converter with magnetic control." in CPSS Transactions on Power Electronics and Applications, vol. 4, no. 4, Dec. 2019, pp. 265-275, doi: 10.24295/CPSSTPEA.2019.00025.
[19] R. Yu, G. K. Y. Ho, B. M. H. Pong, B. W. Ling and J. Lam. "Computer-Aided Design and Optimization of High-Efficiency LLC Series Resonant Converter." in IEEE Transactions on Power Electronics, vol. 27, no. 7, July 2012, pp. 3243-3256, doi: 10.1109/TPEL.2011.2179562.
[20] M. F. Menke, J. P. Duranti, L. Roggia, F. E. Bisogno, R. V. Tambara and Á. R. Seidel. "Analysis and Design of the LLC LED Driver Based on State-Space Representation Direct Time-Domain Solution." in IEEE Transactions on Power Electronics, vol. 35, no. 12, Dec. 2020, pp. 12686-12701, doi: 10.1109/TPEL.2020.2995942.
[21] I. Lee and G. Moon. "Analysis and Design of a Three-Level LLC Series Resonant Converter for High- and Wide-Input-Voltage Applications." in IEEE Transactions on Power Electronics, vol. 27, no. 6, June 2012, pp. 2966-2979, doi: 10.1109/TPEL.2011.2174381.
[22] J. Deng, S. Li, S. Hu, C. C. Mi and R. Ma. "Design Methodology of LLC Resonant Converters for Electric Vehicle Battery Chargers." in IEEE Transactions on Vehicular Technology, vol. 63, no. 4, May 2014, pp. 1581-1592, doi: 10.1109/TVT.2013.2287379.
[23] P. He and A. Khaligh. "Comprehensive Analyses and Comparison of 1 kW Isolated DC–DC Converters for Bidirectional EV Charging Systems." in IEEE Transactions on Transportation Electrification, vol. 3, no. 1, March 2017, pp. 147-156, doi: 10.1109/TTE.2016.2630927.
[24] J. Min and M. Ordonez. "Bidirectional Resonant CLLC Charger for Wide Battery Voltage Range: Asymmetric Parameters Methodology." in IEEE Transactions on Power Electronics, vol. 36, no. 6, June 2021, pp. 6662-6673, doi: 10.1109/TPEL.2020.3033982.
[25] J. Huang, X. Zhang, Z. Shuai, P. Wang, L. H. Koh, and X. Tong. "Robust Circuit Parameters Design for the CLLC-Type DC Transformer in the Hybrid AC–DC Microgrid." in IEEE Transactions on Industrial Electronics, vol. 66, no. 3, March 2019, pp. 1906-1918, doi: 10.1109/TIE.2018.2835373.
[26] P. He, A. Mallik, A. Sankar and A. Khaligh. "Design of a 1-MHz High-Efficiency High-Power-Density Bidirectional GaN-Based CLLC Converter for Electric Vehicles." in IEEE Transactions on Vehicular Technology, vol. 68, no. 1, Jan. 2019, pp. 213-223, doi: 10.1109/TVT.2018.2881276.
[27] W. Chen, P. Rong and Z. Lu. "Snubberless Bidirectional DC–DC Converter With New CLLC Resonant Tank Featuring Minimized Switching Loss." in IEEE Transactions on Industrial Electronics, vol. 57, no. 9, Sept. 2010, pp. 3075-3086, doi: 10.1109/TIE.2009.2037099.
[28] W. Chen, S. Wang, X. Hong, Z. Lu and S. Ye. "Fully soft-switched bidirectional resonant dc-dc converter with a new CLLC tank." 2010 Twenty-Fifth Annual IEEE Applied Power Electronics Conference and Exposition (APEC), 2010, pp. 1238-1242, doi: 10.1109/APEC.2010.5433345.
[29] J. Luo, J. Wang, Z. Fang, J. Shao, and J. Li. (2018). "Optimal Design of a High Efficiency LLC Resonant Converter with a Narrow Frequency Range for Voltage Regulation." Energies, 11(5), 2018, pp. 1124. doi:10.3390/en11051124.
[30] B. Lu, W. Liu, Y. Liang, F. C. Lee and J. D. van Wyk. "Optimal design methodology for LLC resonant converter." Twenty-First Annual IEEE Applied Power Electronics Conference and Exposition, 2006. APEC '06., 2006, pp. 6 pp.-, doi: 10.1109/APEC.2006.1620590.
[31] U. Kundu, K. Yenduri and P. Sensarma. "Accurate ZVS Analysis for Magnetic Design and Efficiency Improvement of Full-Bridge LLC Resonant Converter." in IEEE Transactions on Power Electronics, vol. 32, no. 3, March 2017, pp. 1703-1706, doi: 10.1109/TPEL.2016.2604118.
[32] C. Zhao, Y. -H. Hsieh, F. C. Lee and Q. Li. "Design and Analysis of a High-frequency CLLC Resonant Converter with Medium Voltage insulation for Solid-State-Transformer." 2021 IEEE Applied Power Electronics Conference and Exposition (APEC), 2021, pp. 1638-1642, doi: 10.1109/APEC42165.2021.9487101.

BIOGRAPHIES

BİRAND ERDOĞAN was born in Adana, Turkey, in 1993. He is currently a Ph.D student with the Electrical and Electronics Engineering Department in Çukurova University, Adana. He has been a research assistant with the Electrical and Electronics Engineering Department, Adana Alparslan Türkeş Science and Technology University, since 2019. His current research interests include power electronics, and electric vehicles.

ADNAN TAN was born in Adana, Turkey, in 1985. He received the Ph.D. degree from the Electrical and Electronics Engineering Department, Çukurova University, Adana, in 2015. He has been an Assistant Professor with the Electrical and Electronics Engineering Department, Çukurova University, since 2015. His current research interests include power electronic converters, utility applications of power electronics, electrical power quality, and microgrids.

MURAT MUSTAFA SAVRUN was born in Osmaniye, Turkey, in 1987. He received the Ph.D. degree from the Electrical and Electronics Engineering Department, Çukurova University, Adana, Turkey, in 2017. He has been an Associate Professor with the Electrical and Electronics Engineering Department, Adana Alparslan Türkeş Science and Technology University, since 2022. His current research interests include power electronics, electrical power quality, and electric vehicles.

MEHMET UĞRAS CUMA was born in 1982. He received the B.Sc., M.Sc., and Ph.D. degrees in electrical and electronics engineering from Cukurova University, Adana, Turkey, in 2004, 2006, and 2010, respectively. He is currently an Associate Professor with the Electrical and Electronics Engineering Department, Cukurova University, Adana. His current research interests include power quality, power quality devices, and electric vehicles.

MEHMET TÜMAY received the Ph.D. degree in electrical engineering from Strathclyde University, Glasgow, U.K., in 1995. He is currently a Professor with the Department of Electrical and Electronics Engineering, and the Rector of Adana Alparslan Türkeş Science and Technology University, Adana, Turkey. His current research interests include modeling of electrical machines, power-flow controllers, power quality, and custom power devices.